Bond graph based control using virtual actuators

P J Gawthrop
Centre for Systems and Control and Department of Mechanical Engineering, University of Glasgow, James Watt Building, Glasgow G12 8QQ, Scotland, UK

Abstract: A bond graph based approach to design in the physical domain is described that uses the concepts of virtual actuators and virtual sensors. The approach is illustrated by, and implemented on, an experimental ball and beam system.

Keywords: bond graphs, control systems, real-time control

NOTATION

$C_y(s)$, $C_w(s)$	physical controller transfer functions
e, f	generic effort and flow variables
e_c, f_c	collocated effort and flow at the junction
e_p, f_p	collocated effort and flow at the physical controller
$g_1(s)$, $g_2(s)$	port transfer functions of sub_1 and sub_2
$G_1(s)$	augmented subsystem transfer function between ports
m_b, j_b, m_e	mass, inertia and equivalent mass of the ball
p_o	observer pole position
$r = \sigma$	relative degree of $G_1(s)$
sub_1, sub_2	subsystems of the decomposed system
SCP	shortest causal path
SISO	single input, single output
t	time (s)
u	system input (control signal)
u_2	input to sub_2
V_1, V_2, V_3, V_b	voltages associated with the local controller
w	system setpoint
y_s, y_m, y, y_d	system, model, controlled and desired system outputs
α, $\dot{\alpha}$	beam angle and angular velocity
ζ	damping ratio of the desired model
ρ	ratio of radius to mass centre height of the rolling ball
σ	length of the SCP of sub_1
σ_y, σ_w	length of the SCPs of the physical controller from y to w to u

The MS was received on 1 May 2003 and was accepted after revision for publication on 17 February 2004.

1 INTRODUCTION

Most research into control systems design is conducted in the mathematical domain. One reason for this is to abstract dynamic systems in such a way that control design is generic. Thus, for example, the class of dynamic systems described by linear state-space equations has a well-established set of methods (see, for example, reference [**1**]) that can be applied uniformly to the design of controllers for such systems.

However, it can be argued that this level of abstraction actually distills out system-specific features that could have aided the design procedure using engineering intuition. An alternative approach, 'design in the physical domain', has been suggested by Sharon *et al.* [**2**]. Here, the level of abstraction is a graphical physical representation that lies closer to the system physics than mathematical equations. In particular, the bond graph approach [**3**–**5**] has been suggested [**2**, **6**] as the basis for such design. Moreover, appropriate software tools are now available, including MTT [**7**]. Related model-based work in the robotics area is to be found in the books of An *et al.* [**8**] and Slotine and Li [**9**].

One way of looking at the bond graph based design of controllers is via the use of virtual sensors—the bond graph analogue of observers. Karnopp [**10**] was the first to give a bond graph interpretation of observers, and this idea was extended by Gawthrop *et al.* [**6**, **11**, **12**]. These ideas are particularly fruitful in the context of hierarchical bond graphs [**13**, **14**].

However, the intuitive simplicity of this approach is marred by the fact that, whereas the virtual sensor

concept gives virtual access to the values of all internal signals in the controlled system (whether or not measured directly), it is only possible to access actuators that exist physically. In a similar fashion, the concept of virtual actuators—introduced by Gawthrop *et al.* [**15**]—gives virtual access to the manipulation of internal signals in the controlled system (whether or not actuated directly).

The virtual actuator approach is related to the celebrated backstepping approach of Krstic *et al.* [**16**]. In particular, Yeh [**17**] has given a bond graph interpretation of the celebrated backstepping approach of Krstic *et al.* [**16**]. The material presented by Yeh [**17**] can be interpreted as an approach to design in the physical domain using virtual actuators and as such provided an important impetus for this paper. However, this work is complemented in a number of ways, including:

(a) embedding the approach into a virtual sensor approach,
(b) using the ideas of bicausal bond graphs [**18**] and system inversion [**19**–**21**] to generate the virtual actuators,
(c) applying the virtual actuator approach to a laboratory electromechanical system.

This paper focuses on linear systems, although the essential features are applicable to the non-linear case.

The outline of the paper is as follows. Section 2 provides a summary of the physical model based control approach, and section 3 describes the virtual actuator approach together with an introductory example. Section 4 provides a detailed account of the bond graph modelling of the experimental system, and section 5 shows how the virtual actuator approach can be designed and applied in this case. Section 6 gives some experimental results that both illustrate and validate the approach. Section 7 concludes the paper.

2 PHYSICAL MODEL BASED CONTROL

Figure 1 shows the basic ideas of physical model based control [**6**, **11**, **12**]. In particular, Fig. 1 has three main parts:

(a) a physical model of the system, typically expressed as a bond graph,
(b) observer feedback, again expressed in bond graph terms [**10**],
(c) controller feedback.

These three interconnected subsystems, driven by the system output y_s and setpoint w, provide and control signal u and can be viewed as a two-degree-of-freedom compensator.

Because the model is implemented as a simulation within the compensator, sensor access to the signals y_i on all junctions is available. As discussed elsewhere [**6**, **10**], the purpose of the observer feedback is to drive all signals

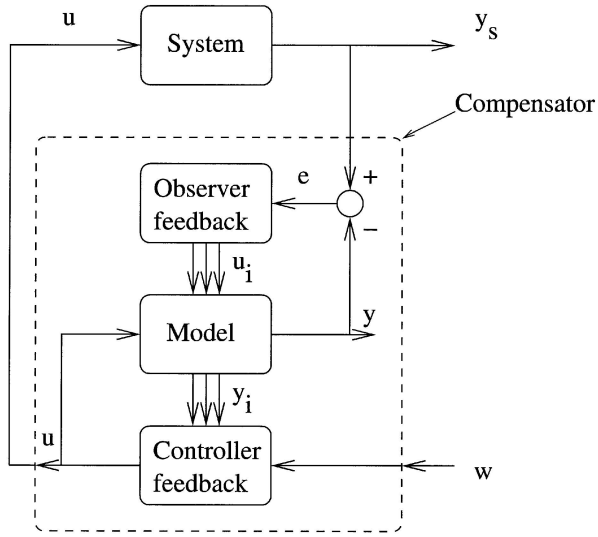

Fig. 1 Physical model based control

within the model towards those in the system itself. Thus, the model junctions provide virtual access to system junctions, and thus the controller feedback (item c) can make use of these virtual sensors.

If a control signal and the corresponding control output are bond graph covariables on the same bond, the sensor and actuator are said to be collocated. As discussed in the bond graph context by Gawthrop [**6**], and in the control-theoretic context by Slotine and Li [**9**], collocated controllers are easier to design than non-collocated controllers. In particular, the controller can be constructed out of purely passive elements and can be viewed as the attachment of a passive physical system described by a bond graph to the appropriate junction [**6**].

The contribution of this paper is to show how, in addition to these virtual sensors, virtual actuators can be used to simplify the design of the controller component (item c) of Fig. 1.

3 VIRTUAL ACTUATOR CONTROL

As discussed in section 2, Fig. 1 shows the basic ideas of physical model based control [**6**]; this section focuses on a new approach for designing the controller part. In particular, the controller can be designed as if a passive physical system could be attached to a junction, even though neither of the collocated effort/flow pair is available; the previously developed virtual sensor concept provides the measurement, and the virtual actuator of this section provides access to the control covariable. The virtual source/sensor pair is provided by a corresponding virtual junction.

Like the related backstepping approach [**16**, **17**], virtual actuator control is only possible for a restricted set of systems. In particular, the following assumptions are required.

Assumption 1

The system model of Fig. 1 can be decomposed into two two-port subsystems, sub_1 and sub_2, connected by a 1 junction if the system controlled output y is a flow (or a 0 junction if y is an effort), where y is the common covariable of the junction and u is the input to sub_1. Subsystem sub_2 imposes y on to the connection junction.

Assumption 2

The SISO augmented system of Fig. 3a comprising the system sub_1 with an effort amplifier (AE) appended to the output if y is an effort [or a flow amplifier (AF) appended to the output if y is a flow] has a stable inverse.

Figure 2a shows the situation described in Assumption 1 in the particular case where both $y = f_c$ and u are flows and e_c and f_c are the pair of effort and flow covariables associated with the system output y. Assumption 2 can be verified in a number of ways including direct inversion of the bond graph [**18**–**20**, **22**–**28**]. In the linear case, Assumption 2 has a transfer function interpretation. In particular, if $G_1(s)$ is the SISO transfer function of the augmented system, then Assumption 2 is equivalent to the requirement that all zeros of $G_1(s)$ have a strictly negative real part.

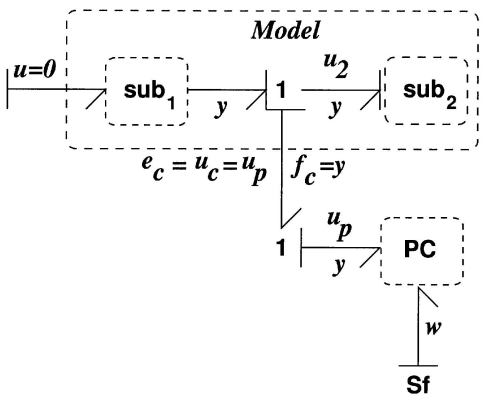

(a) Equivalent control

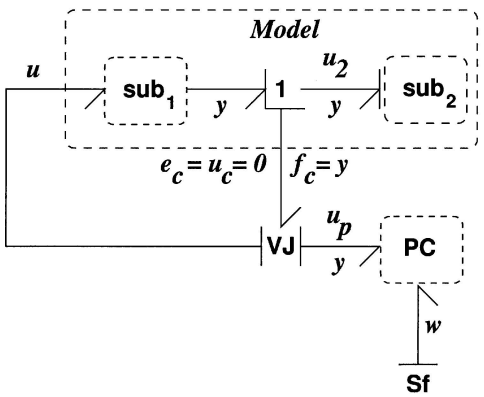

(b) Virtual junction

Fig. 2 Virtual actuator control

As well as Assumptions 1 and 2, some structural information about the augmented system of Assumption 2 is required. In particular, the length of the shortest causal path (SCP) σ [**19**] from the input to the output is required. In the linear case the length of the SCP is the same as the relative degree r of the transfer function $G_1(s)$, $r = \sigma$.

In view of the discussion of section 2, the virtual actuator design procedure has two steps:

1. With reference to Fig. 2a, choose a physical controller (PC) as if the collocated effort/flow pair e_c and f_c were both available and the system input $u = 0$.
2. With reference to Fig. 2b, choose the (dynamic) three-port virtual junction component (VJ) such that

$$\begin{cases} e_c = 0 & \text{if } y = f_c \\ f_c = 0 & \text{if } y = e_c \end{cases} \tag{1}$$

and u is such that the transfer function relating y and w is the same using the collocated control of Fig. 2a and the virtual actuator control of Fig. 2b.

These two steps are considered in sections 3.1 and 3.2 and illustrated in section 3.3.

3.1 Virtual junction

The purpose of the virtual junction (VJ) in Fig. 2b is to make the controlled model output y the same as that in Fig. 2a. The assumption of linearity allows a simple transfer function approach to this design. With reference to Fig. 2a, the relevant equations are

$$\begin{cases} u_2 = g_1(s)y - u_p & \text{sub}_1 \text{ and junction} \\ y = g_2(s)u_2 & \text{sub}_2 \\ u_p = C_w(s)w - C_y(s)y & \text{physical controller} \end{cases} \tag{2}$$

where $g_1(s)$ and $g_2(s)$ are the transfer functions relating the collocated pairs on the ports of sub_1 and sub_2 connected to the connecting junction, and $C_y(s)$ and $C_w(s)$ are the transfer functions relating the model output y and the setpoint w to the control signal u_p.

Similarly, the corresponding equations relating to Fig. 2b are

$$\begin{cases} u_2 = g_1(s)y + G_1(s)u & \text{sub}_1 \text{ and junction} \\ y = g_2(s)u_2 & \text{sub}_2 \\ u_p = C_w(s)w - C_y(s)y & \text{physical controller} \end{cases} \tag{3}$$

It follows that the equations of the virtual junction are

$$\begin{aligned} u &= G_1^{-1}(s)u_p \\ u_c &= 0 \end{aligned} \tag{4}$$

It is clear that the virtual junction requires inversion of the transfer function $G_1(s)$ and thus inversion of the augmented subsystem of Fig. 3a. The bond graph interpretation of inversion is now well established [**18**–**20**, **22**–**28**]. In particular, Ngwompo and Gawthrop [**20**] consider the situation where an inverted subsystem is embedded within a larger system in such a way that the overall system can be realized in state-space form; that is, in the linear case, the overall system transfer function is proper even when the inverted subsystem is improper. A method developed by Ngwompo and Gawthrop [**20**, section 4.2] is used to give a bond graph interpretation of the virtual junction.

Figure 3b shows the application of this method [**20**, section 4.2] to the creation of a virtual junction. This is based on the configuration of Fig. 2 which has a 1 junction separating sub_1 and sub_2. The VJ component corresponding to a 0 junction is obtained by replacing 0 junctions by 1 junctions and vice versa.

As mentioned previously, the VJ component has three ports:

(a) the port connected to the separating junction which passes the flow signal y to the physical controller PC while imposing a zero effort signal $u_c = 0$;
(b) the port connected to the input of sub_1 which passes the appropriate control signal u to the model input;
(c) the port connected to the physical controller.

As discussed by Ngwompo and Gawthrop [**20**, section 4.2], the bicausal (see Appendix 8) zero-effort and zero-flow source SS:z (see Appendix 8) has the effect of both forcing the effort on the attached 0 junction to be zero but also forcing the flows above and below the attached 0 junction to be the same. The bicausal effort and flow sensor SS:sink makes sure that, externally, the VJ component has normal causality. The augmented subsystem component aug_sub_1 is effectively inverted by the impinging bicausal bonds.

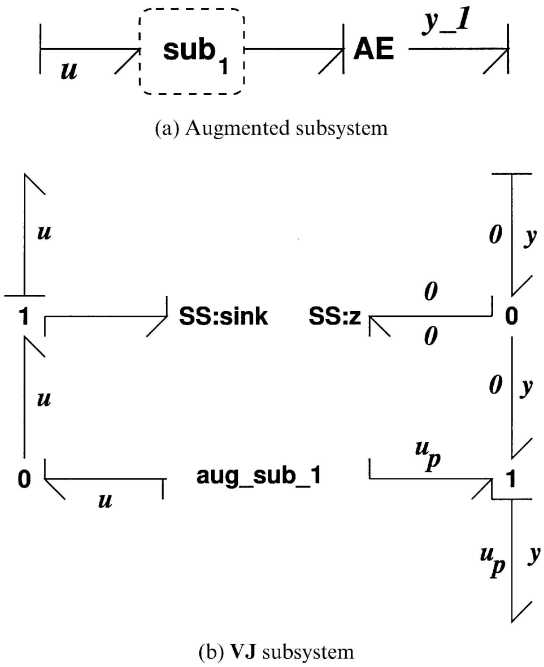

Fig. 3 Virtual junction

3.2 Physical controller

As discussed by Gawthrop [**6**], the physical controller for the collocated sensor/actuator pair can be designed in the physical domain using engineering judgement and intuition. This is exemplified in sections 3.3 and 5. However, the use of the virtual actuator approach means that the following design restriction must be applied.

Design Rule 1

Defining σ_w as the length of the shortest causal path (SCP) between w and u_p and σ_y as the length of the SCP between y and u_p, then

$$\sigma_y \geqslant \sigma$$
$$\sigma_w \geqslant \sigma \tag{5}$$

From Fig. 3b, these two inequalities imply that the transfer functions relating y and w to u are proper.

3.3 Example: two coupled tanks

Figure 4 shows a simple hydraulic system comprising two tanks of liquid in series; the input u is the inflow to the first tank and the controlled output y is the pressure at the base of the second tank. For illustrative simplicity, it is assumed that $r_1 = r_2 = 1$ and $c_1 = c_2 = 1$.

Figure 5a is in the same form as Fig. 2a and shows the decomposition of Assumption 1. It can readily be shown that the corresponding transfer function is

$$G_1(s) = \frac{y}{u} = \frac{1}{1+s} \tag{6}$$

This transfer function has a relative degree $r = 1$ and therefore an SCP length of $\sigma = 1$. It has no inverse dynamics, and therefore Assumption 2 is also satisfied.

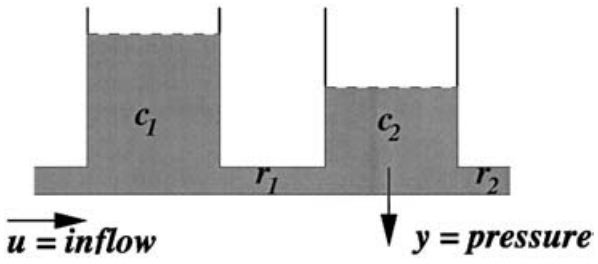

Fig. 4 Example: two coupled tanks

I04203 © IMechE 2004

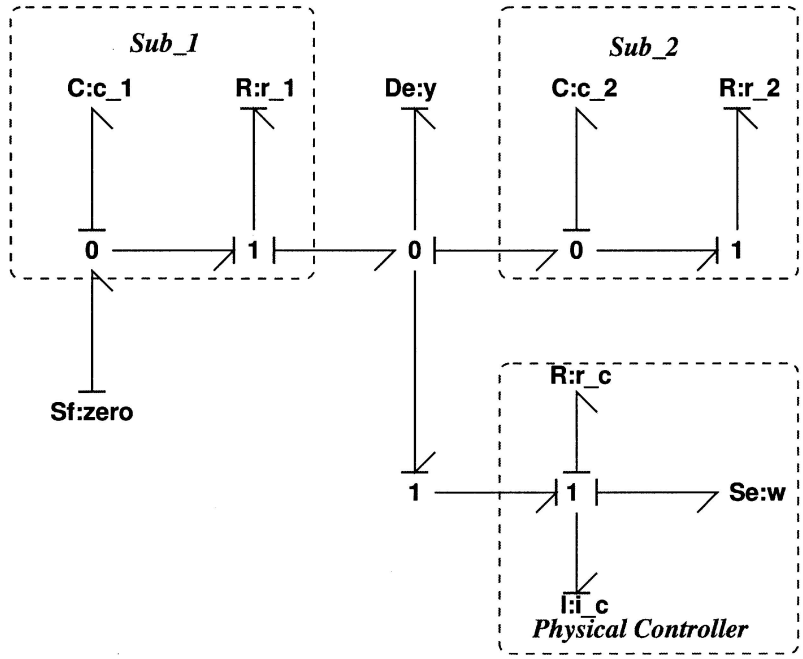

(a) Equivalent control

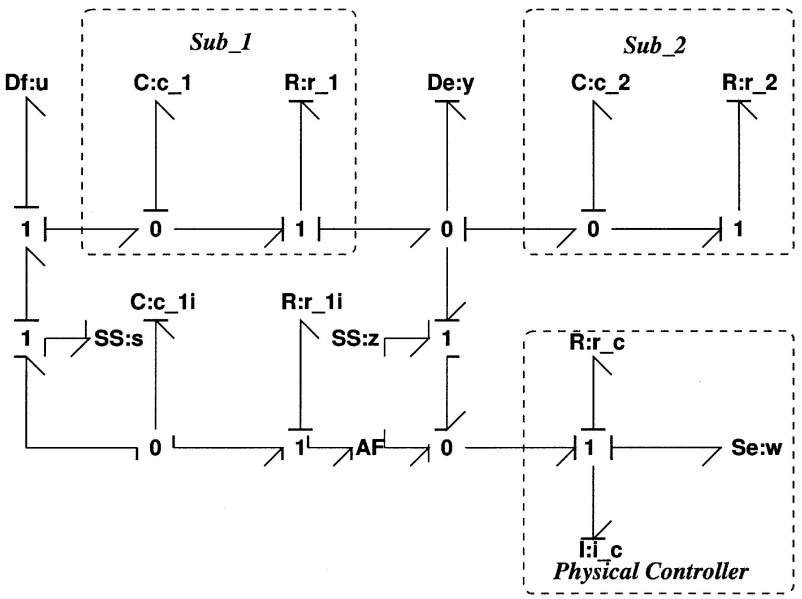

(b) Virtual junction

Fig. 5 Virtual actuator control: example

The physical controller PC has been chosen to have SCP lengths $\sigma_w = \sigma_y = 1$, thus satisfying Design Rule 1. In fact, the transfer function is

$$u = \frac{1}{i_c s + r_c}(w - y) \tag{7}$$

The closed-loop transfer function corresponding to Fig. 5a is

$$y = \frac{s+1}{i_c s^3 + (3i_c + r_c)s^2 + (i_c + 3r_c + 1)s + r_c + 1} w \tag{8}$$

The relative degree of this transfer function is 2, the same as that of the open-loop system.

Figure 5b shows the virtual actuator version of Fig. 5a. The closed-loop transfer function relating y and w is, of course, that of equation (8). That giving the control signal u is

$$u = \frac{s^3 + 4s^2 + 4s + 1}{i_c s^3 + (3i_c + r_c)s^2 + (i_c + 3r_c + 1)s + r_c + 1} w \qquad (9)$$

This is the proper transfer function, illustrating the fact that, although the design method includes inversion, the controller itself is proper. Figure 6 shows the unit step response of y (firm line) and u (dashed line) for particular values of the parameters.

The design of the compensator (Fig. 1) involves observer design as well as controller design; this is not pursued further here. An example of observer design appears in section 5.2.

4 SYSTEM MODELLING

The experimental system was a Quanser Consulting ball and beam experiment [**29**, section 2.2] (with a modified connecting cable as described below). Figure 7 shows the overall arrangement with the power supply (universal power module) on the left, the ball and beam in the centre and the controlling computer on the right. Figures 10a and 11a show more detail of the ball and beam arrangement.

An accurate model of the system is required to build the controller. As discussed in the following sections, engineering judgement was used to reduce the order of the models of some of the subsystems.

4.1 Drive subsystem

The Quanser SRV-R2 drive is used to actuate the system. It comprises a d.c. motor, gearing and a potentiometer measuring angle.

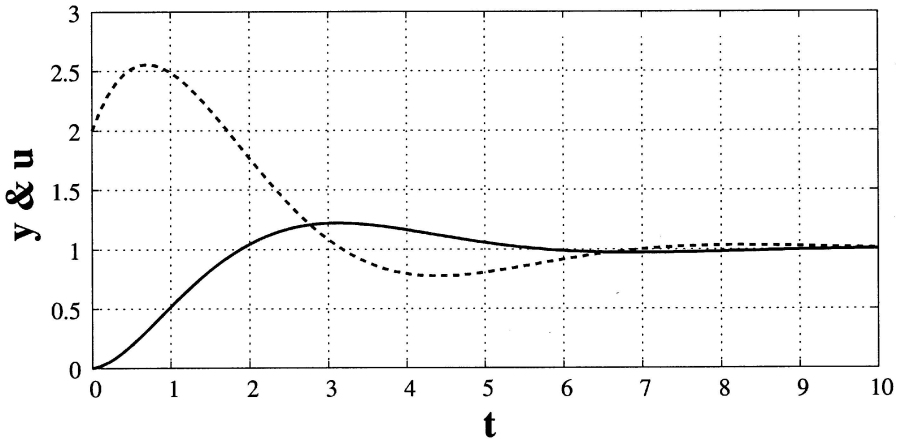

Fig. 6 Example: step response $r_c = 0$, $i_c = 0.5$

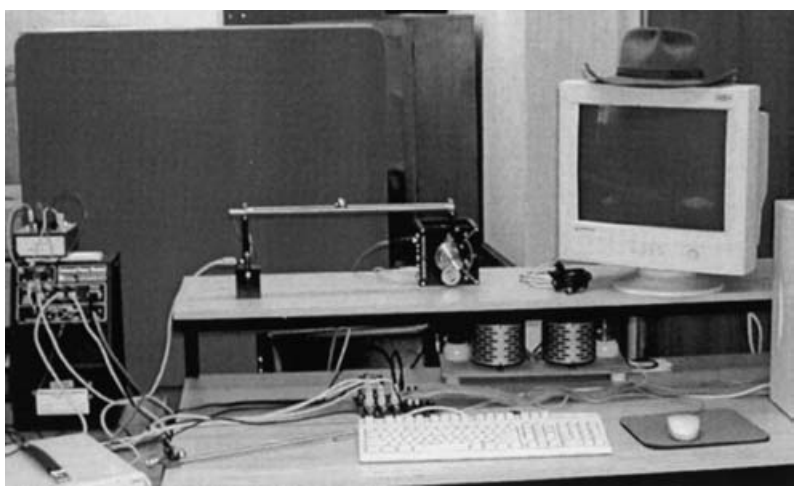

Fig. 7 Ball and beam apparatus

I04203 © IMechE 2004

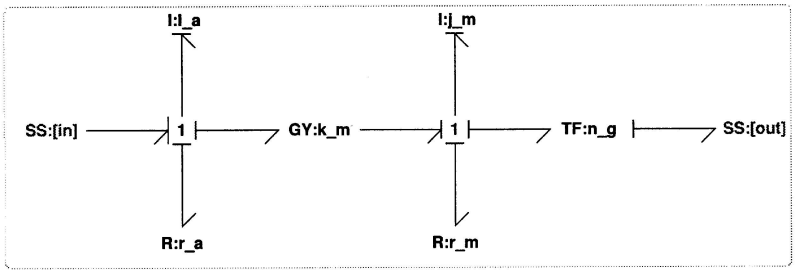

(a) Bond Graph

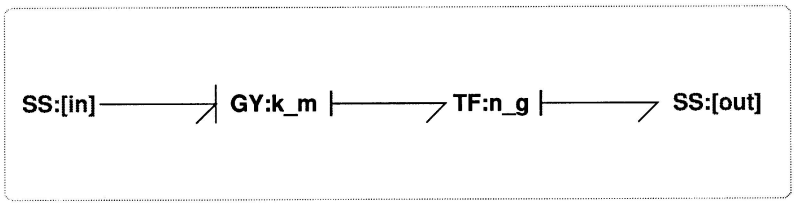

(b) Reduced Bond Graph

Fig. 8 Drive subsystem

The bond graph of Fig. 8a shows the main system components, and Table 1 gives the corresponding description and parameter values. The unloaded system has two poles at about $s = -47$ and $s = -14397$ and, because of the large gear ratio n_g, external loading has a negligible effect. Given the time constants of the inner-loop controller of section 4.5, the dynamic components corresponding to both these poles can then be removed. Again, the large gear ratio means that the motor torque (and hence armature current) is small and thus the armature resistance R : r_a may also be removed.

Hence, the reduced bond graph of Fig. 8b is used in the sequel. In essence, this gives a non-dynamical relation between shaft angular velocity ω and input voltage u

$$\omega = \frac{1}{k_m n_g} u \tag{10}$$

4.2 Power electronics

The d.c. motor described in section 4.1 is driven by a Quanser universal power module (UPM) type 1503 [**29**].

Table 1 Drive subsystem

Component	Description	Parameter value
R : r_a	Armature resistance	$r_a = 2.6\ \Omega$
I : I_a	Armature inductance	$l_a = 0.16$ mH
GY : k_m	Electromechanical conversion	$k_m = 0.00767$ nm/A
I : j_m	Armature + gear inertia	$j_a = 4.87 \times 10^{-7}$ kg m^2
TF : n_g	Torque-amplifying gear ratio	$n_g = 70$

The cable supplied by Quanser contains feedback resistors; this was replaced by an ordinary cable so that the UPM power operational amplifier could be directly patched.

As shown in Fig. 9a, three resistors were used to provide a two-input power amplifier from the UPM. Using the approach of Gawthrop and Palmer [**30**], the bond graph of Fig. 9b was constructed to represent the modified UPM. The corresponding two-input, one-output amplifier can be written as

$$V_2 = \frac{r_1 r_2 + r_2 r_3 + r_3 r_1}{r_2 r_3} V_0 - \frac{r_1}{r_3} V_1 \tag{11}$$

As discussed in section 4.5, V_1 is used to provide feedback from a voltage measurement V_b. This is a high-impedance sensor that is therefore buffered by an amplifier. The equation is

$$V_1 = g_a V_b \tag{12}$$

The values of the various parameters appear in Table 2.

4.3 Beam subsystem

Figure 10a shows the schematic diagram of the beam and the connected subsystems: the motor drive (section 4.1)

Table 2 Power electronic component values

Component	Description	Parameter value
R : r_1	Op-amp feedback resistor	$r_1 = 5$ kΩ
R : r_2	Op-amp earth resistor	$r_2 = 5$ kΩ
R : r_3	Op-amp input resistor	$r_3 = 10$ kΩ
AE : g_a	Sensor buffer amplifier	$g_a = 10$

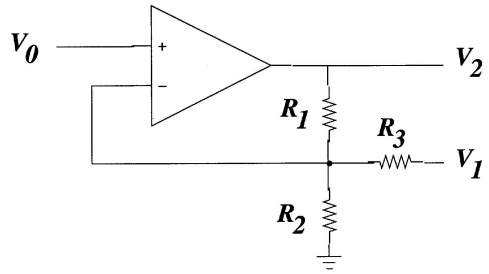

(a) Schematic

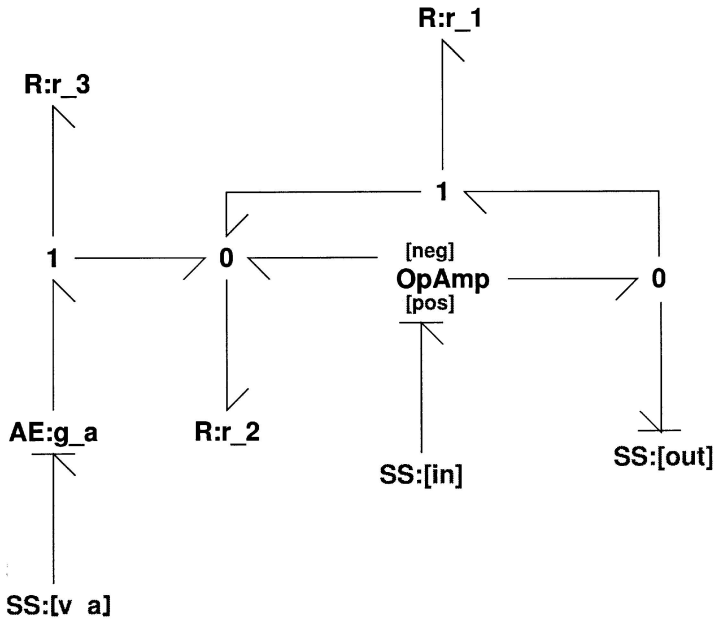

(b) Bond Graph

Fig. 9 Universal power module

and the ball (section 4.4). The beam is connected to the drive output gear via a connecting rod and set up such that, when the drive angle $\theta = 0$, the beam angle $\alpha = 0$ and the connecting rod is vertical. For small angles, it follows that

$$\alpha = n_b \theta \tag{13}$$

where $n_b = l_g/l_b$; differentiating with respect to time, $\dot{\alpha} = n_b \dot{\theta}$. The force acting on the ball in the direction of the beam is $f_b = m_e g \sin(\alpha)$. For small values of α, this can be approximated by $f_b = m_e g \alpha$. It is convenient to define the normalized force

$$F = \frac{f_b}{m_e} = g\alpha \tag{14}$$

F and $\dot{\alpha}$ can be regarded as the effort/flow pair associated with a C component.

According to the Quanser manual [**29**], the angular inertia of the beam is $j_b = 0.0029\ \text{kg m}^2$. When referred to the motor, the equivalent inertia is $j_{be} = j_b/n_g^2 = 5.9 \times 10^{-7}\ \text{kg m}^2$. As discussed in section 4.1, this can be neglected.

Figure 10b shows the bond graph of the beam. The components are described in Table 3.

4.4 Ball subsystem

Figure 11a gives the schematic diagram of a spherical ball rolling (without slipping) on a pair of rails. The ball radius is r and the height of the centre of mass above the rails is h. Note that, if the ball were rolling on a plane, $r = h$; with reference to Fig. 11a, this is not the case here because the ball protrudes beneath the rails.

Table 3 Beam subsystem

Component	Description	Parameter value
TF : n_b	Transforms $\dot{\theta}$ to $\dot{\alpha}$ [equation (13)]	$n_b = \frac{l_g}{l_b} = \frac{0.0254}{0.4318} = 0.05882$
C : g	Gives F from $\dot{\alpha}$ [equation (14)]	$g = 9.81\ \text{m/s}^2$

I04203 © IMechE 2004

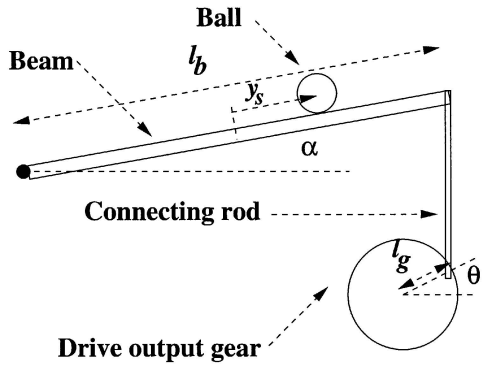

(a) Schematic

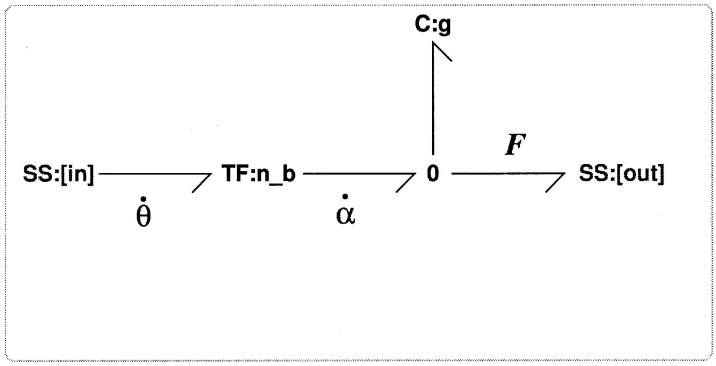

(b) Bond Graph

Fig. 10 Beam subsystem

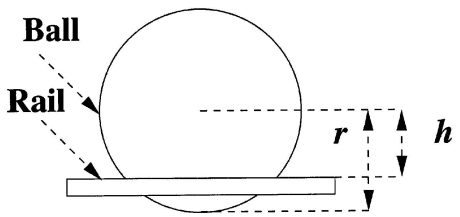

(a) Schematic

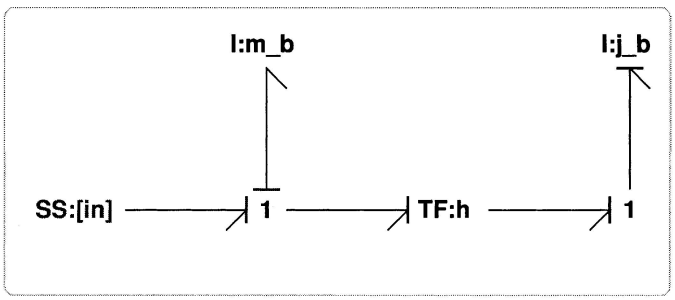

(b) Bond Graph

Fig. 11 Ball subsystem

There are two forms of motion associated with the ball: linear motion in the direction of the rails and rotational motion about the centre of mass. These motions are coupled by the no-slippage condition: the ball velocity v_b and angular velocity ω_b are related by $v_b = h\omega_b$.

Figure 11b gives a bond graph describing this situation; the components are described in Table 4. Only one of the I components can be in integral causality; one choice is given in Fig. 11b. In effect, the system dynamics correspond to a single I component representing linear

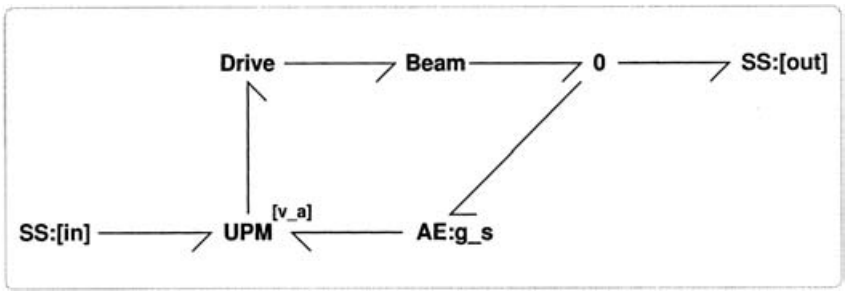

Fig. 12 Inner control loop bond graph

Table 4 Ball subsystem

Component	Description	Parameter value
I : m_b	Ball mass (linear motion)	Mass $= m_b$(kg)
I : j_b	Ball rotational inertia (rotational motion)	$j_b = \frac{2/5}{m_b} r^2$, $r = 12.5$ mm
TF : h	Transforms linear to rotational motion	$h = 7.5$ mm

motion with an equivalent mass m_e given by

$$m_e = (1 + \tfrac{2}{5}\rho^2)m_b \tag{15}$$

where $\rho = r/h$. In this case $\rho = 12.5/7.5 = 5/3$, giving $m_e = 2.11 m_b$.

In the Quanser manual [**29**], the value is given as $m_e = \frac{7}{5} m_b = 1.4 m_b$; this is presumably based on the incorrect assumption that $r = h$.

4.5 Inner-loop controller

Use of the virtual actuator approach does not preclude conventional control methods as part of the overall scheme. In particular, as a reliable measurement of beam angle (via a geared potentiometer) was available, a simple proportional controller was used to control the beam angle. This controller was patched as described in section 4.2. The corresponding bond graph appears in Fig. 12.

The virtual actuator based controller was then cascaded with this controller. Thus, u is the setpoint to the inner loop.

5 COMPENSATOR DESIGN

With reference to Fig. 2, sub_1 is the UPM, drive and beam and local controller subsystem given in the bond graph of Fig. 12, and sub_2 is the ball subsystem of Fig. 11b. The compensator design then comprises the desired model (section 5.1) and the observer design (section 5.2). The compensator implementation via the virtual junction approach is then accomplished by software as described in section 5.3.

5.1 Desired model

Bringing engineering insight to bear on controller design is a motivation for physical model based control. The purpose of the ball and beam controller is to make the ball position y (Fig. 10a) follow a desired value w. A physical approach to this is to attach a spring to the ball and have the other end of the spring as the desired position; damping would be added using a dashpot to avoid simple harmonic motion.

Figure 13a shows a schematic diagram of such a physical controller, where w is the position of the right-hand end of the spring (measured in m) and F is the force acting on the ball attached to the left-hand end of the spring (measured in N). The reason for having the left-hand spring k_1 is to satisfy Design Rule 1; i.e. the force on the spring is not applied as soon as w changes. However, k_1 can be much larger that k_2. The values used appear in Table 5. Ignoring the stiff spring k_1, these

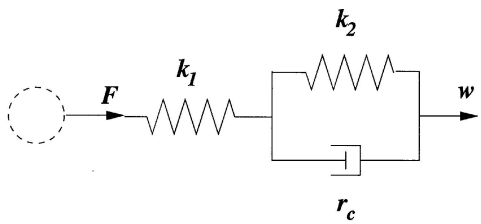

(a) Schematic

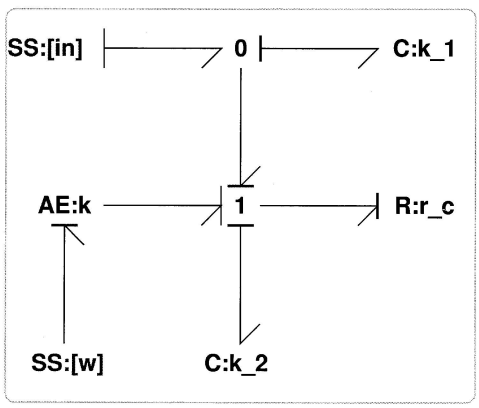

(b) Bond Graph

Fig. 13 Physical controller

I04203 © IMechE 2004

Table 5 Physical controller

Component	Description	Parameter value
C : k_1	Stiff spring	$k_1 = 100$ N/m
C : k_2	Spring	$k_2 = 4.987$ N/m
R : r_c	Dashpot	$r_c = 6.333$ N/m s

values correspond to a closed-loop natural frequency $\omega_n = 1.5$ rad/s and a damping ratio $\zeta = 1$; this latter value was changed on-line during the experiment, as discussed in section 5.3. The corresponding bond graph appears in Fig. 13b, and the components are explained in Table 5.

This controller cannot be implemented directly as there is no way to apply $u_p = F$ directly to the ball, and the covariable (the velocity of the ball $y = \mathrm{d}y_s/\mathrm{d}t$) is not available for measurement. The former problem is overcome using the virtual actuator approach; the latter is overcome using an observer-based position measurement y_s.

5.2 Observer design

Observer design is well known in the context of state-space systems [**1**]. In the context of bond graphs it was initiated by Karnopp [**10**] and further discussed in the context of physical model based control by Gawthrop [**6**], and so only the application-specific details are given here.

The dynamic system from control input u to measured output y_s is fourth order. The observer gains were determined by a pole placement method to give four coincident real poles at $s = -p_o$. The observer pole position p_o was adjusted on-line during the experiments.

5.3 Real-time software

The virtual actuator controller was implanted on an Intel-based computer equipped with a Quanser-supplied A/D D/A card and running the RTLinux version of real-time Linux [**31**] with the COMEDI data acquisition software [**32**]. The software providing a graphical user interface, data collection and real-time control was written for the real-time laboratory at the University of New South Wales (UNSW).

The controller equations were automatically generated using the bond graph toolbox [**7**]. MTT is based on symbolic algebra, and it was therefore possible to generate the code partly numerically and partly symbolically. In particular, all parameters except the observer pole location p_o and the damping ratio ζ were resolved numerically. This gave a simple code while allowing these two parameters to be adjusted on-line. In addition, the equations for the desired response y_d were also generated on-line to provide a comparison between the actual output y_s and the desired output y_d.

6 EXPERIMENTAL RESULTS

Using the equipment depicted in Fig. 7, a number of experiments were conducted in the real-time control laboratory of the University of New South Wales. The experimental sequence reported here was performed on 16 November 2002.

One run, lasting approximately 380 s, was recorded, and the data are plotted in Fig. 14. The figure has three subplots:

(a) the system output (ball position) plotted as a firm line, together with the setpoint (dotted line) and the output of the desired model (dashed line);
(b) the system input (the voltage read into the UPM) measured in volts;
(c) two normalized parameters: the damping ratio ζ of the desired model (firm line) and the observer pole location $p_o/20$ (dotted line)

In each case, the data are plotted against time measured in seconds. For a time greater than about $t = 220$ s, the setpoint is zero, but the system was subjected to a sequence of disturbances effected by manually tapping the ball so that it moved away from the zero position towards the maximum position of about ± 0.2 m $= 200$ mm.

Figures 16 and 17 show expanded versions of Fig. 14 for specific time ranges. These figures are used to clarify a number of points relating to the experimental evaluation of the methods of this paper.

As discussed in section 5.3, two parameters (the damping ratio ζ and the observer pole parameter p_o) were left as symbols in the code. Using the shared memory interface, these could be adjusted on-line; part (c) of each figure shows how they were varied throughout the experiment. The following subsections focus on specific aspects of these experimental results.

6.1 Tracking offsets

A glance at Fig. 14 shows that the steady state value of the actual ball position is not always the same as the corresponding desired value; there is a constant offset. The effect is most marked in the time range of Fig. 15. In particular, the offsets at times of 15 and 25 s are listed in Table 6. Closer inspection of Fig. 15 reveals that the offset is associated with a corresponding non-zero control signal. Again, the control signals are listed in Table 6. In other words, at these particular times, the beam has a constant tilt yet the ball is stationary.

Table 6 Constant offsets

Time (s)	Offset (mm)	Control signal (V)
15	21	−0.16
25	−14	0.10

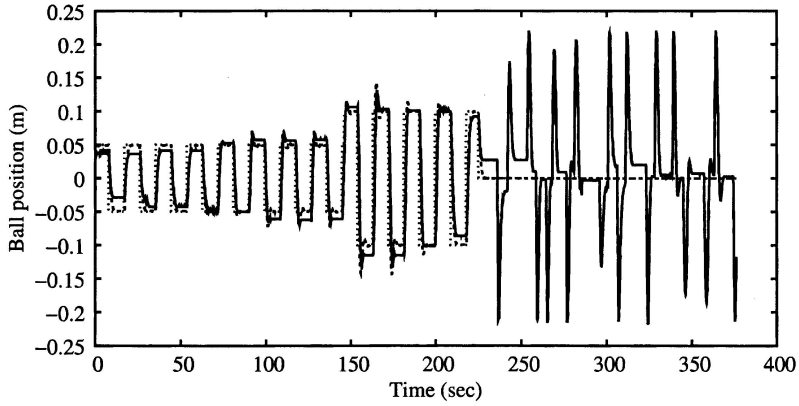

(a) Output, desired output and setpoint

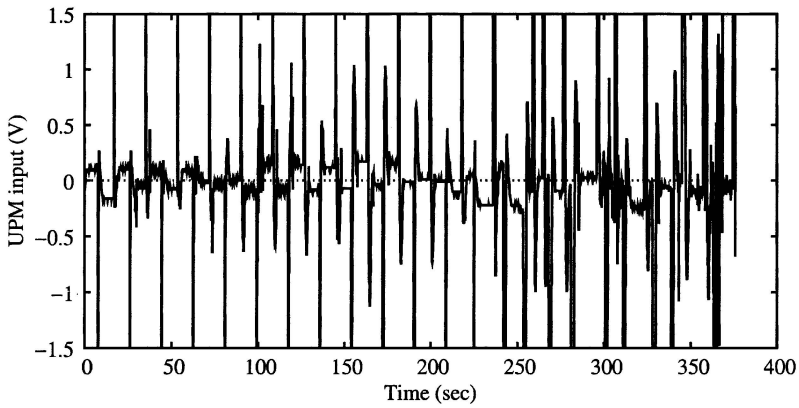

(b) Control signal

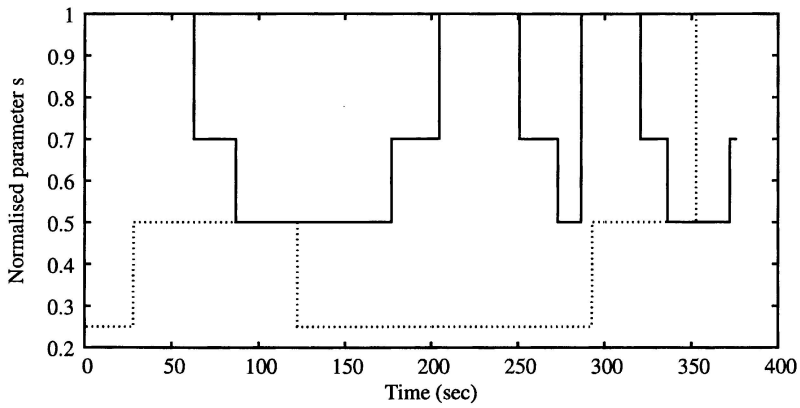

(c) ζ and $\frac{p_0}{20}$

Fig. 14 Entire dataset

Examination of Fig. 11 shows that, as in practice the ball has a non-zero contact area, there will be a certain amount of rubbing between the ball and rail. It is postulated that this rubbing gives rise to static friction and hence the ball can be stationary on a tilted beam. This postulate also explains the fact that, when the desired system is critically damped (as in Figs 15 and 16 for $t > 205$ s), the ball comes to rest below the setpoint, whereas for the overdamped desired system (as in Fig. 16 for $t < 176$ s) the ball comes to rest beyond the setpoint.

I04203 © IMechE 2004

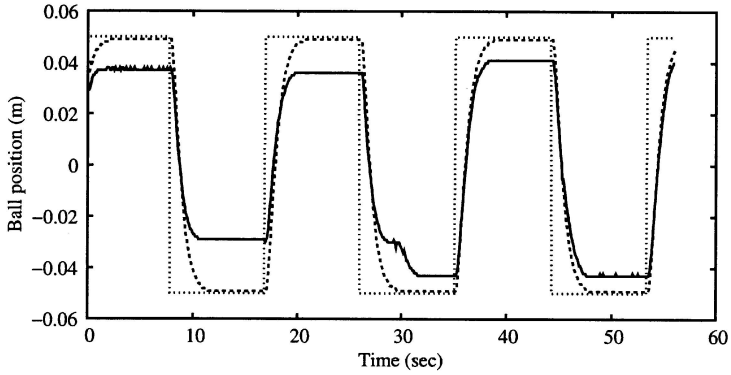

(a) Output, desired output and setpoint

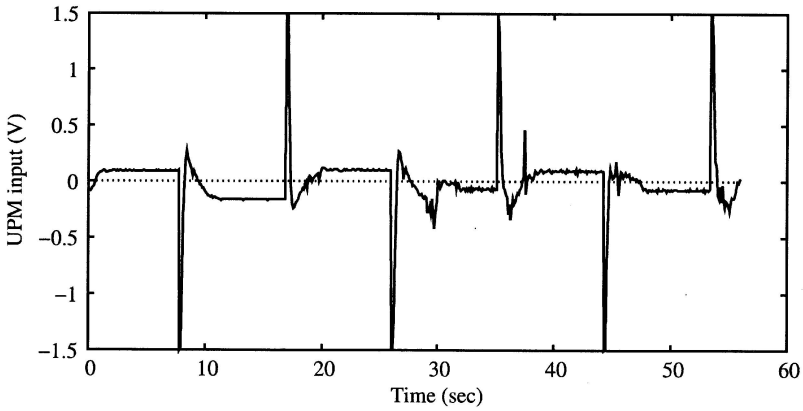

(b) Control signal

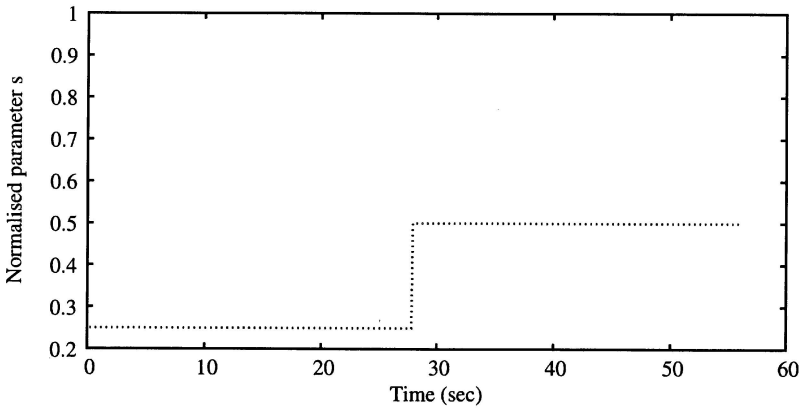

(c) ζ and $\frac{p_0}{20}$

Fig. 15 Setpoint following ($\zeta = 1$): vary observer pole p_o

This friction effect is neglected in the model of the rolling ball of section 4.4. It is therefore not surprising that the actual closed-loop system behaves as the desired closed-loop system of section 5.1 with the addition of the neglected friction effect.

Figure 15 is selected to show the 'worst' of this effect; in particular, the setpoint value is quite small (± 0.05 m $= 50$ mm) and the desired model is critically damped, and thus the desired output approached the setpoint slowly. In contrast, Fig. 16 shows the situation

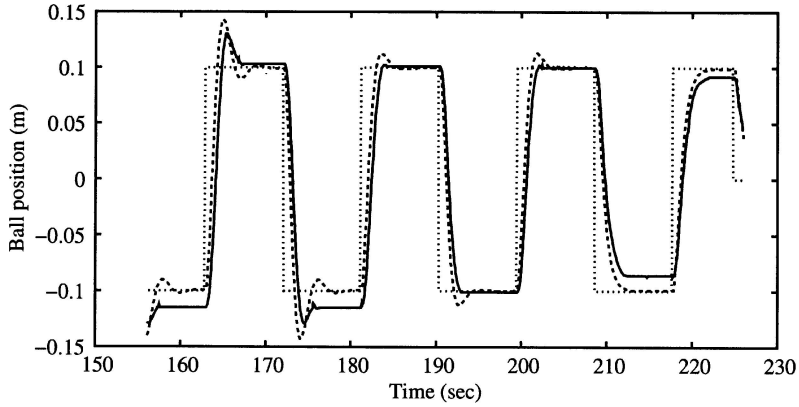

(a) Output, desired output and setpoint

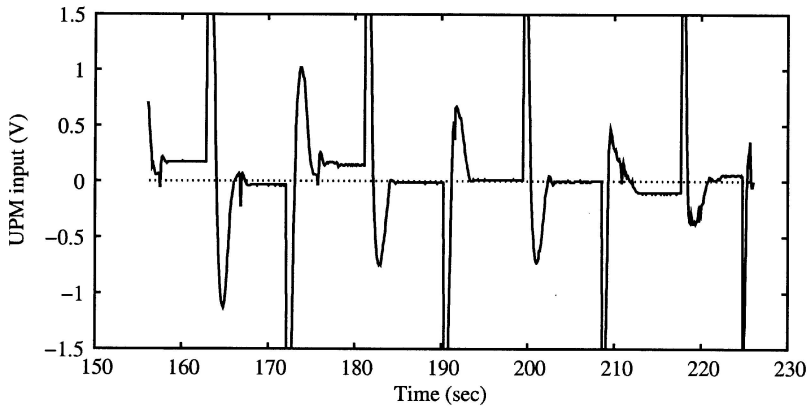

(b) Control signal

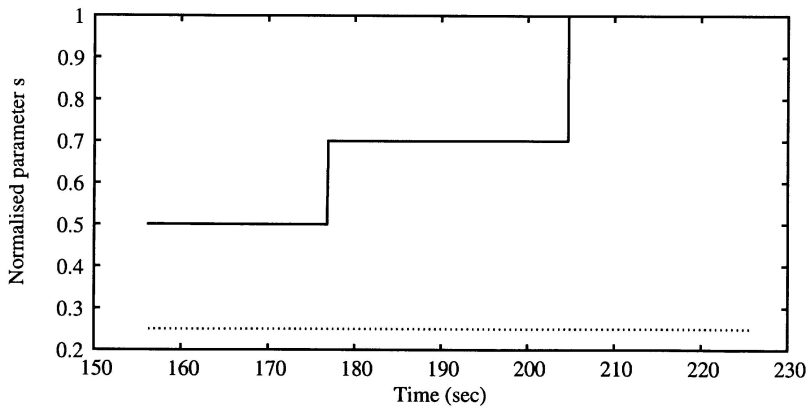

(c) ζ and $\frac{p_0}{20}$

Fig. 16 Setpoint following: vary damping ratio ζ

where the setpoint is larger (± 0.1 m $= 100$ mm) and, initially, the desired model is underdamped. Here, the effect of the postulated friction is less in both absolute and relative terms. Section 7 suggests some modifications to the desired model to overcome this effect.

6.2 Varying the pole position p_o

As discussed in section 5.2, the choice of observer poles has no effect on the setpoint response but does affect the response to disturbances and measurement noise.

Examination of Fig. 15c shows that the observer pole position has the value

$$p_o = \begin{cases} 5, & t < 28 \text{ s} \\ 10, & t > 28 \text{ s} \end{cases} \quad (16)$$

Figure 15a confirms that the setpoint response is broadly unchanged by the change in pole position, whereas Fig. 15b shows that measurement noise is amplified more when the pole position increases at time $t = 28$ s. The reduction in offset (see section 6.1) after time $t = 28$ s

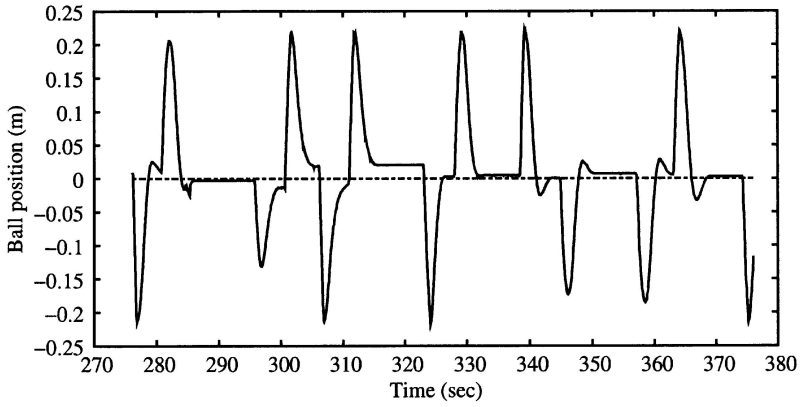

(a) Output, desired output and setpoint

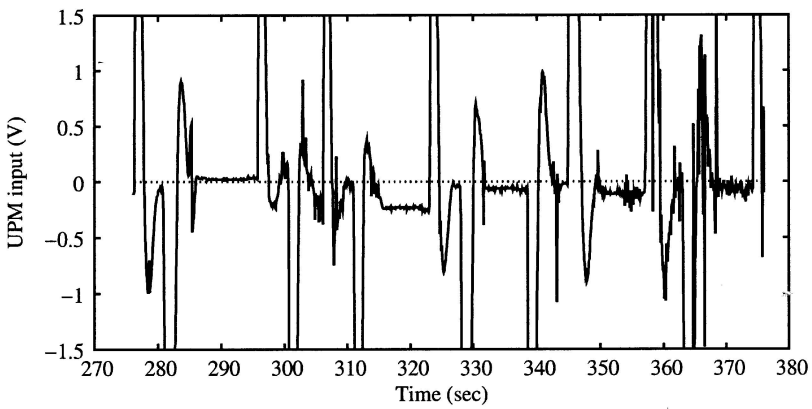

(b) Control signal

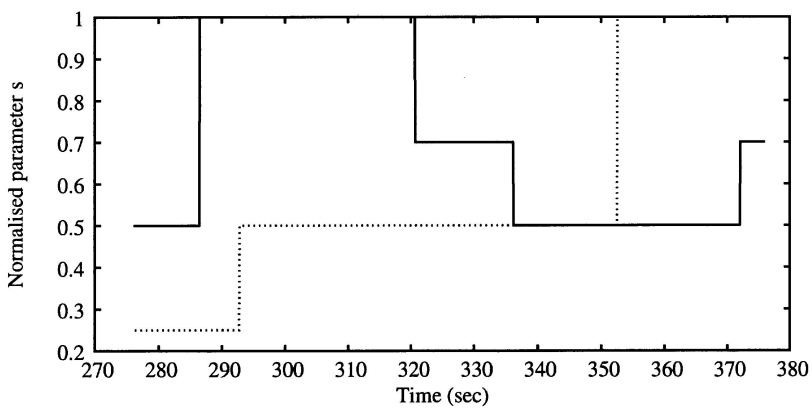

(c) ζ and $\frac{p_0}{20}$

Fig. 17 Regulation: vary both parameters

is attributed to the 'jitter' effect of the increased noise component of the control signal.

The setpoint remains at zero throughout Fig. 17. Again, the increase in the noise component of the control signal with increasing p_o can be clearly seen, together with the reduction in offset. The final value of $p_o = 10$ leads to quite large values of noise in the control signal; p_o was not increased further for fear of damaging the motor.

The purpose of the observer is to extract the ball velocity $v = dy/dt$ from the ball position y (Fig. 11). As the pole position increases, the observer output becomes a closer approximation to v; this explains the noise amplification arising from large values of p_o.

6.3 Varying the damping ratio ζ

Figure 16 focuses on the effect of varying the damping ratio ζ. Examination of Fig. 16c shows that the damping ratio has the value

$$\zeta = \begin{cases} 0.5, & 155 < t < 177 \text{ s} \\ \dfrac{1}{\sqrt{2}}, & 177 < t < 205\text{s} \\ 1, & 205 < t < 225 \text{ s} \end{cases} \quad (17)$$

The dotted line of Fig. 16a shows the output y_d of the desired model which reflects the damping ratios listed in equation (17). Moreover, the system output y (the firm line of Fig. 16a) follows y_d closely, apart from the offset mentioned in section 6.1.

6.4 Disturbance rejection

During the time period of Fig. 17, the controller setpoint was set to zero, but the system was disturbed by repeatedly tapping the ball so that it moved away from the zero position towards the maximum position of about ± 0.2 m $= 200$ mm. Figure 17a shows that the controller successfully regulates the system output y (ball position) back towards zero after each disturbance.

7 CONCLUSION

A new approach to physical model based control using virtual actuators has been introduced and illustrated using a simple example. This controller allows design as if a collocated input–output pair were available to attach a passive physical system; thus, engineering insight from the appropriate physical domain can be brought to bear directly on the control design problem.

A detailed design of a controller for a physical system—the Quanser 'ball and beam' apparatus—has been accomplished to illustrate the approach.

An experimental evaluation of the design has been discussed that shows that, apart from the static friction effect discussed in section 6.1, the controller behaves as expected.

There are a number of approaches that could be used to eliminate the static friction effect, including lubrication of the rolling ball, using a non-linear spring in the desired model and deliberately introducing jitter into the control signal.

The discussion is limited to linear models; further work will examine the case of non-linear models.

ACKNOWLEDGEMENTS

The work described here was accomplished while the author was a Visiting Professor at the University of New South Wales within the Systems and Control Research Group of the School of Electrical Engineering and Telecommunications. He acknowledges the support and facilities provided by Professor V. Solo and the theoretical and practical help provided by Dr David Clements, Dr Ray Eaton and Chris Lu. The author is grateful to the anonymous referees who made many helpful suggestions for improving the clarity of this paper.

REFERENCES

1 **Kwakernaak, H.** and **Sivan, R.** *Linear Optimal Control Systems*, 1972 (John Wiley).
2 **Sharon, A., Hogan, N.** and **Hardt, D. E.** Controller design in the physical domain. *J. Franklin Inst.*, 1991, **328**(5), 697–721.
3 **Karnopp, D., Margolis, D. L.** and **Rosenberg, R. C.** System Dynamics: Modeling and Simulation of Mechatronic Systems, 3rd edition, January 2000 (Horizon Publishers and Distributors).
4 **Cellier, F. E.** *Continuous System Modelling*, 1991 (Springer-Verlag, Berlin, Germany).
5 **Gawthrop, P. J.** and **Smith, L. P. S.** *Metamodelling: Bond Graphs and Dynamic Systems*, 1996 (Prentice-Hall, Hemel Hempstead).
6 **Gawthrop, P. J.** Physical model-based control: a bond graph approach. *J. Franklin Inst.*, 1995, **332B**(3), 285–305.
7 MTT: model transformation tools. Online www home page, 2002, URL: http://mtt.sourceforge.net.
8 **An, C. H., Atkeson, C. G.** and **Hollerbach, J. M.** *Model-based Control of Robot Manipulators*, 1988 (The MIT Press, Cambridge, Massachusetts).
9 **Slotine, J. E.** and **Li, W.** *Applied Nonlinear Control*, 1991 (Prentice-Hall, Englewood Cliffs, New Jersey).
10 **Karnopp, D. C.** Bond graphs in control: physical state variables and observers. *J. Franklin Inst.*, 1979, **308**(3), 221–234.
11 **Roberts, D. W., Ballance, D. J.** and **Gawthrop, P. J.** Design and implementation of a bond graph observer for robot control. *Control Engng Pract.*, October 1995, **3**(10), 1447–1457.

 I04203 © IMechE 2004

12 **Gawthrop, P. J.** and **Ponton, J. W.** Improved control using dynamic process models. *Chem. Engng Res. Des.*, January 1996, **74**(A1), 63–69.
13 **Gawthrop, P. J.** and **Ballance, D. J.** *Symbolic Computation for Manipulation of Hierachical Bond Graphs*, number 56 in Control Engineering Series, 1999, Ch. 2, pp. 23–51 (IEE, Stevenage).
14 **Gawthrop, P. J.** and **Ballance, D. J.** Symbolic algebra and physical-model-based control. *Computing and Control J.*, April 1997, **8**(2), 70–76.
15 **Gawthrop, P. J., Ballance, D. J.** and **Vink, D.** Bond graph based control with virtual actuators. In Proceedings of 13th European Simulation Symposium on *Simulation in Industry* (Eds N. Giambiasi and C. Frydman), Marseille, France, October 2001, pp. 813–817 (SCS).
16 **Krstic, M., Kanellakopoulos, I.** and **Kokotovic, P. V.** *Nonlinear and Adaptive Control Design*, 1995 (John Wiley, New York).
17 **Yeh, T.-J.** Backstepping control in the physical domain. *J. Franklin Inst.*, 2001, **338**, 455–479.
18 **Gawthrop, P. J.** Bicausal bond graphs. In Proceedings of International Conference on *Bond Graph Modeling and Simulation* (*ICBGM'95*) (Eds F. E. Cellier and J. J. Granda), Las Vegas, Nevada, January 1995, Vol. 27 of Simulation Series, pp. 83–88 (Society for Computer Simulation).
19 **Ngwompo, R. F., Scavarda, S.** and **Thomasset, D.** Inversion of linear time-invariant siso systems modelled by bond graph. *J. Franklin Inst.*, 1996, **333B**(2), 157–174.
20 **Ngwompo, R. F.** and **Gawthrop, P. J.** Bond graph based simulation of nonlinear inverse systems using physical performance specifications. *J. Franklin Inst.*, November 1999, **336**(8), 1225–1247.
21 **Gawthrop, P. J.** Physical interpretation of inverse dynamics using bicausal bond graphs. *J. Franklin Inst.*, 2000, **337**(6), 743–769.
22 **Gawthrop, P. J.** Control system configuration: inversion and bicausal bond graphs. In Proceedings of 1997 International Conference on *Bond Graph Modeling and Simulation* (*ICBGM'97*) (Eds J. J. Granda and G. Dauphin-Tanguy), Phoenix, Arizona, January 1997, Vol. 29 of Simulation Series, pp. 97–102.
23 **Ngwompo, R. F.** Contribution au dimensionnement des systèms sur des critières dynamiques et énergétiques—approche par bond graph. PhD thesis, INSA de Lyon, 1997.
24 **Ngwompo, R. F., Scavarda, S.** and **Thomasset, D.** Physical model-based inversion in control systems design using bond graph representation. Part 1: theory. *Proc. Instn Mech. Engrs, Part 1: J. Systems and Control Engineering*, April 2001, **215**(I2), 95–103.
25 **Ngwompo, R. F., Scavarda, S.** and **Thomasset, D.** Physical model-based inversion in control systems design using bond graph representation. Part 2: applications. *Proc. Instn Mech. Engrs, Part 1: J. Systems and Control Engineering*, 2001, **215**(I2), 105–112.
26 **Wu, S. T.** and **Youcef-Toumi, K.** On the relative degrees and zero dynamics from physical system modelling. *Trans. ASME, J. Dynamic Syst., Measmt and Control*, 1995, **117**(2), 1–13.
27 **Huang, S. Y.** and **Youcef-Toumi, K.** Zero dynamics from bond graph models. Part i: SISO systems. *Trans. ASME, J. Dynamic Syst., Measmt and Control*, March 1999, **121**(1), 10–17.
28 **Huang, S. Y.** and **Youcef-Toumi, K.** Zero dynamics from bond graph models. Part ii: MIMO systems. *Trans. ASME, J. Dynamic Syst., Measmt and Control*, March 1999, **121**(1), 18–26.
29 **Apkarian, J.** *A Comprehensive and Modular Laboratory for Control Systems Design and Implementation*, 1995 (Quanser Consulting).
30 **Gawthrop, P. J.** and **Palmer, D.** A bicausal bond graph representation of operational amplifiers. *Proc. Instn Mech. Engrs, Part 1: J. Systems and Control Engineering*, 2003, **217**(I1), 49–58.
31 RT-Linux. Real-Time Linux Home Site. Online www home page, 2000, http://www.rtlinux.org/rtlinux.
32 Comedi. Comedi Home Site. Online www home page, 2002, http://www.comedi.org/.

APPENDIX

Bicausal bond graphs

Bicausal bond graphs were introduced in reference [**18**] to give a foundation for deriving system properties directly from the system bond graph that relate to:

(a) system inversion,
(b) state estimation,
(c) parameter estimation.

Following reference [**21**], this paper utilizes the first of these: system inversion.

As discussed in reference [**18**], the two bicausal bonds appearing in Fig. 18a correspond to the following pairs of equations respectively

$$e_2 = e_1, \qquad f_2 = f_1 \tag{18}$$

$$e_1 = e_2, \qquad f_1 = f_2 \tag{19}$$

In other words, the notation is such that:

1. A causal half-stroke on the flow side of the bond (the common convention that the half-arrow is on the flow side of the bond is adopted) implies that flow is imposed on the variable associated with the far end of the bond (the variable associated with the far end of the bond is on the left-hand side of the assignment statement).
2. A causal half-stroke on the effort side of the bond implies that effort is imposed on the variable associated with the near end of the bond (the variable associated with the near end of the bond is on the left-hand side of the assignment statement).

Source-sensor component

Traditionally, the S_e and S_f components have a special status among bond graph components in that the corresponding causality is irrevocably fixed; this causes problems in the context of this paper. In addition, they are sometimes used to represent the measurement of the corresponding flow and effort respectively.

These components are not used in this paper, but, as discussed in reference [**18**] they are replaced by the source-sensor (SS) component of Fig. 18a. Figure 18a shows the four possible bicausal versions. In order they imply effort source/flow sensor, flow source/effort sensor, flow and effort source and flow and effort sensor.

Amplifier component

The AE component was introduced in reference [**5**] as a replacement for an active bond; it is required in the context of this paper to correctly display bicausality. There are two causal patterns used in this paper which are displayed in Fig. 18b. The upper part of the figure, corresponding to normal causality, corresponds to the two assignment statements

$$e_2 = e_1, \qquad f_1 = 0 \tag{20}$$

The lower part of the figure, corresponding to bicausality, corresponds to the two assignment statements

$$e_1 = e_2, \qquad f_1 = 0 \tag{21}$$

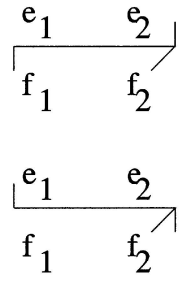

(a) Bicausal bonds

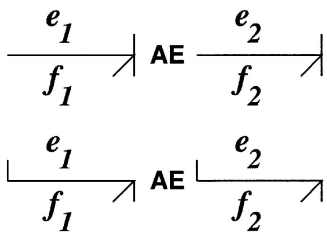

(b) Effort amplifier component

Fig. 18 Bond graph extensions

I04203 © IMechE 2004